Scien. Tech. Bull-Chem. Food Sci. Eng., Vol. 17 (XVIII), 2020, 32-39

ZR(IV) MOFS BASED ON TEREPHTALIC ACID AND ACETIC ACID MODULATOR

Mirela PICIORUS, Alexandru POPA, Catalin IANASI, Elisabeta I. SZERB, Carmen CRETU*

"Coriolan Dragulescu" Institute of Chemistry, Romanian Academy, 24 Mihai Viteazu Bvd., 300223 Timisoara, Romania
Corresponding author email: carmencretu78@gmail.com

Abstract: *Herein, we present the investigation of a fast modulated synthesis of micro/meso sized ZrMOF, porous materials known as UIO-66, containing terephtalic acid (H_2BDC) as organic linker using an excess of metal salt precursor and different concentrations of acetic acid (AAc) as organic modulator. The increase in the concentration of modulator up to a certain value leads to an improvement of surface area and a modification of pore structure by producing mesopores at the expense of micropores.*

Keywords: Zirconium (IV) Metal-organic frameworks; terephtalic acid; surface area

INTRODUCTION

Metal-organic frameworks (MOFs) are an innovative class of crystalline porous materials constructed from metal nodes or clusters coordinated by organic linkers into two-dimensional or three-dimensional extended periodic network structures (Chen et al. 2019, Sharmin et al. 2016). These compounds have attracted much interest in recent years, due to i) their structural and topological characteristics and ii) for large area of applications based on their large internal surface area, permanent porosities, tunable pores, as well as their versatile functionalities (Li et al. 2016, Fang et al. 2018). Different combinations of metals and organic binders may provide an infinite number of MOFs structures with distinct physico-chemical properties (Bai et al. 2016). The type of metal centre (ion radius, coordination number, electron configuration), interaction/ distances between the metal ions, the coordination ability of the ligand and the ligand shape (bend, length, and substituents) controls the entire structure topology (Xiong et a. 2016). Different types of carboxylate ligands, flexible and rigid ones, are employed in the construction of MOFs (Wang et al. 2015), though the aromatic rigid dicarboxylate ligands have been extensively used due to the stability and permanent porosity of the resulting materials (Angeli et al. 2020). Other factors with relevance in the MOFs architecture are metal-to-ligand molar ratios, solvent and reaction temperatures, counter ions and pH values of the reaction systems, etc (Seetharaj et al. 2019, Yao et al. 2019, Li et al. 2017, Winarta et al. 2020).

ZrMOFs are one of the most studied porous materials based on their high porosity, exceptional thermal, structural and water stability, with versatile potential applications, including gas storage (Ghanbari et al. 2020), molecule adsorption (Chang et al. 2020, Guan et al. 2020), catalysis (Su et al. 2020, Kirlikovali et al. 2020), drug delivery (Jiang et al. 2019), luminescence biosensing (Liu et al. 2020), molecular recognition (Wang et al. 2019) and so on. The enhanced stability of ZrMOFs can be attributed to the strength of the Zr-O coordination bonds caused by acid-hard base interactions between Zr (IV) atoms and oxygen atoms (Drout et al. 2019). The first ZrMOFs (UIO-66 series) based on terephtalic acid derivative were reported by Cavka and colaborators (Cavka et al. 2008), wherein $Zr_6O_4(OH)_4$ octahedral secondary building units (SBUs) link twelve linear dicarboxylate linkers, each in three dimensions to form a highly porous structure and high structural resistance against water and external mechanical pressure (Kalaj et al. 2020, Han et al. 2018). The obtaining of large single crystal or compact polycrystalline films are hard to achieve. Thus, in this direction, numerous studies have been showed that the inclusion of monocarboxylic acids as modulators, into the synthesis of zirconium MOFs can help the crystallization of the final product (Feng et al. 2015) by slowing down

the crystal formation or can affect it turning in a gel-like amorphous product (Hu et al. 2015). Schaate et *al.* (Schaate et al. 2011) have shown the importance of choosing of a proper type and amount of modulator and maintaining an equilibrium exchange between the modulator and dicarboxylic acid used in order to control the crystallite and particle sizes of the product. Moreover, the modulator or the linker can promote the formation of defects in the MOF structure, followed by an increase in the surface area and pore volume (Helal et al. 2020) with a positive impact in applications such as gas adsorption and catalysis (Taddei 2017, Ren et al. 2017)

Since the MOF architecture is greatly dependent on the metal-to-ligand molar ratios and the majority of the studies are based on a 1 to 1 molar ratio, we chose to investigate the modulator influence in metal precursor excess synthesis condition respectively in a 1.5 to 1 metal-to-ligand ratio. Accordingly, herein we report the investigation of a fast modulated synthesis of micro/meso sized ZrMOF porous materials containing terephtalic acid as organic linker, excess of Zr salt precursor and different concentration of acetic acid (AAc) as organic modulator.

MATERIALS AND METHODS

All commercially available reagents and solvents were of analytical grade and used without further purification. Zirconium oxychloride octahydrate ($ZrOCl_2 \cdot 8H_2O$), N,N-dimethylformamide (DMF) were purchased from Riedel de Haën, terephtalic acid (H_2BDC) and ethanol (EtOH) were from Sigma Aldrich, and acetic acid (CH_3COOH) was purchased from Silal Trading. Infrared spectra (KBr) in the range 4000–400 cm^{-1} were recorded on a Cary 630 FT-IR spectrophotometer. Thermal analysis curves were obtained in the temperature range of 25-800 °C (heating rate of 10 °C/min) using a TGA/SDTA 851/LF/1100 Mettler Toledo thermo-gravimetric analyzer. The experiments were conducted under a nitrogen flow of 50 mL/min and dynamic atmosphere of air introduced at 800 °C followed by a final isothermal heating for 15 min. The samples with mass of about 10–20 mg were placed in alumina crucible of 150 mL. The textural parameters were obtained by using Surface Area & Pore Size Analyzer Quantachrome Nova 1200e apparatus. In order to prepare the material for analysis, the samples were degassed under vacuum for 17 h at 100ºC. The N_2 adsorption-desorption isotherms were acquired using 44 point in the 0.05-1 P/Po interval at 77K. Using a NovaWin software, the surface area was determined using BET (Brunauer, Emmett, Teller) (Brunauer et al. 1938) and the total pore volume was determined from the last point which is closest to 1P/Po. The pore size distribution (PSD) was determined by DFT method using the calculation model: N_2 at 77 K on carbon for slit pore with NL-DFT (Non-Local Density-functional theory) equilibrium model (Ravikovitch et al. 1995). This method is specific for microporosity not just mesoporosity.

Synthesis

The synthesis of zirconium-dicarboxylate MOFs noted as ZrMOF_equivalents of acetic acid, was based on a previously reported procedure with some amendments (Chen et al. 2018). ZrMOFs were prepared *in a closed bottom flask* by heating solutions containing zirconium salts as precursor, terephtalic acid as ligand, and acetic acid as a modulator.

General method: Terephtalic acid (400 mg, 2.4 mmol), $ZrOCl_2 \cdot 8H_2O$ (1150 mg, 3.5 mmol), acetic acid (amounts of AAc: 0 mL for ZrMOF_0eq; 2.65 mL, 46 mmol for ZrMOF_13eq; 5.3 mL, 92 mmol for ZrMOF_26eq; 10.6 mL, 185 mmol for ZrMOF_52eq; 21.2 mL, 370 mmol for ZrMOF_104eq), DMF (18 mL) were combined in a 50 mL borosilicate glass, sealed and heated to 120°C for 24 h. The solution was cooled at room temperature. The white polycrystalline powders were collected by filtration and air dried. As-synthesized samples were washed with 10 mL of DMF two times/day during three days and immersed in ethanol, followed the same procedure as washing in DMF. The solid was then dried at 160°C under vacuum for 12 h to yield activated sample.

RESULTS AND DISCUSSIONS

All ZrMOFs reported here were obtained keeping constant the solvent volume and the molar ratio between terephtalic acid and zirconium salt (1:1.5) and increasing the amount of AAc from 0 to 104 molar equivalents. Similar studies were reported on ZrMOFs based on terephtalic (UIO-66) using different metal-ligand molar ratio and various types/amount of modulator (Li et al. 2016, Schaate et al. 2011, Han et al. 2015).

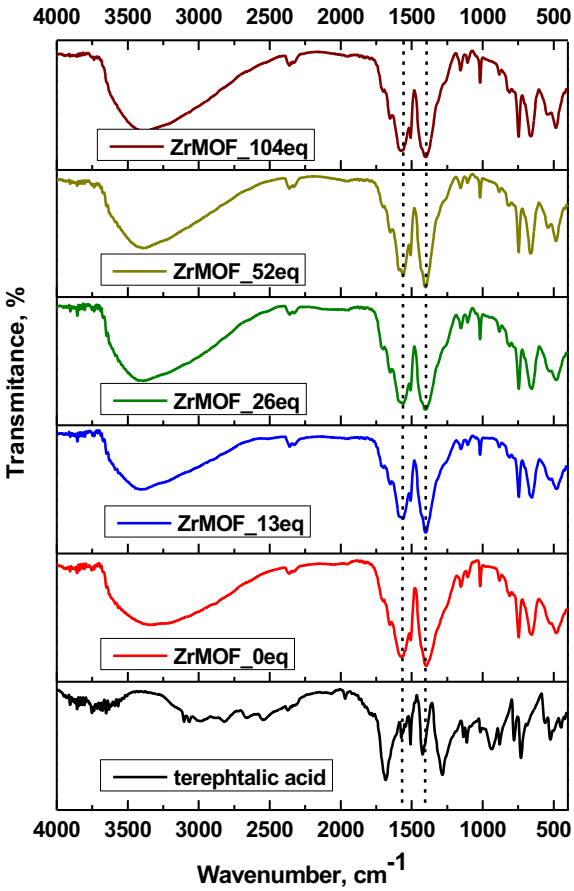

Figure 1. FT-IR spectra of the ZrMOFs samples with different amount of AAc vacuum dried at 160°C.

The FT-IR spectra of the samples (Figure 1) reveal the presence of coordinated carboxylate groups by the asymmetric and symmetric stretching vibrations found around 1580 cm^{-1} and 1400 cm^{-1}, respectively (Yang et al. 2018) when compared with the free ligand presenting only one band at 1680 cm^{-1}. The bands around 1660 cm^{-1} observed in all samples can be attributed to the stretching modes of the carbonyl group (C=O) of the DMF residues trapped inside the pores (Winarta et al. 2020). The bands in the range 1156-1100 cm^{-1} and 781-482 cm^{-1} are assigned to the C-H in-plan and out-of-plane ring bending, respectively (Silverstein et al. 1998). The bands found in the range 661-653 cm^{-1} are attributed to asymmetric vibration of the Zr-(μ_3-O) bridges in the framework building blocks (Piszczek et al. 2007) and the band around 500 cm^{-1} is associated with the stretching vibration of Zr-(OC) bonds (Wang et al. 2017).

The thermal decomposition of the activated ZrMOFs was investigated in dynamic nitrogen atmosphere from ambient temperature to 800°C when air dynamic atmosphere was introduced followed by an isothermal heating for 15 minutes (Figure 2).

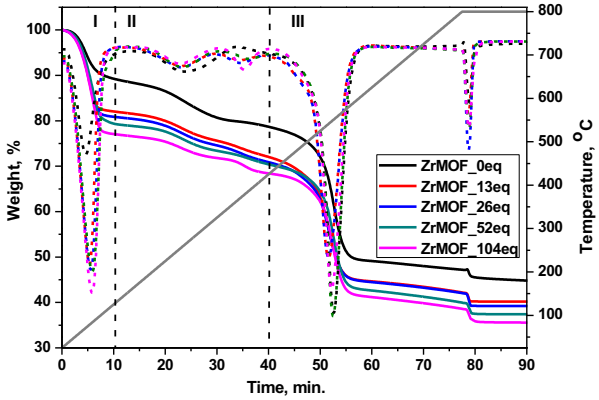

Figure 2. TGA (solid line) and DTG (short dash line) curves of the activated ZrMOFs.

All samples have been vacuum dried at 160°C; however, they are highly hygroscopic when kept in air atmosphere. The TG/DTG curves revealed three important weight loss steps highlighted on DTG curve by intense and well delimited peaks (first and third steps) and broad peaks (second step) (Table1). The first step in the curve was in the range of temperature from 25°C to 150°C and can be attributed to the loss of the physisorbed water. The weight loss of water increases from the free acetic acid sample to the sample with highest content of modulator as follows: 11,58% (ZrMOF_0eq) < 18.29% (ZrMOF_13eq) < 19.44% (ZrMOF_26eq) < 21.06% (ZrMOF_52eq) < 23.35% (ZrMOF_104eq). The increased capacity to retain water can be explained by the changes of the porous structure and surface area (Pan et al. 1996). The second step, up to 420°C, contain two not well resolved weight losses associated with the dehydroxylation of the

metal node (ca. 150-330°C), and removal of acetic acid (ca. 330-420°C) (Ardila-Suarez et al. 2019). In the third step, starting with 420°C the decomposition of the linker (terephtalic acid) took place, followed by the obtaining of ZrO_2 residue, after complete degradation of the organic moiety at 800°C.

Table 1. Temperature of decomposition stages on DTG tomograms and the content of ZrO_2

Samples	*T_{peak} [°C]*			*Residuum [%]*
	1st step	*2nd step*	*3th step*	*ZrO_2*
ZrMOF_0eq	*67.8*	*262.0*	*550.6* *800.0*	*44.87*
ZrMOF_13eq	*73.9*	*255.2* *368.8*	*540.7* *800.0*	*40.20*
ZrMOF_26eq	*75.4*	*256.4* *369.6*	*540.5* *800.0*	*39.44*
ZrMOF_52eq	*79.7*	*258.7* *385.9*	*550.7* *800.0*	*37.26*
ZrMOF_104eq	*78.9*	*252.5* *379.2*	*547.2* *800.0*	*35.56*

T_{peak}, DTG peak temperature (maximum change of weight)

Based on the fact that ideal (defect-free) (dehydroxylated) UiO-66 ZrMOF has the formula $Zr_6O_6(BDC)_6$, the values of weight loss (%) between 420 and 800°C (after desolvation, dehydroxylation, and modulator loss) allow us to estimate a number of 3.47, 3.17, 3.12, 3.25, 3.25 ligands in each unit of ZrMOF_0eq, ZrMOF_13eq, ZrMOF_26eq, ZrMOF_52eq and ZrMOF_104eq (Li et al. 2016). The large number of missing linker could be explained by a possible competition between the linker and DMF/modulator (with the same chemical functionality as the linker) to bind the metal node resulting in sample with missing linker or cluster defects (Han et al. 2015, Shearer et al. 2016, Winarta et al. 2020). The decrease of the percent of remaining ZrO_2 residue with increasing of modulator amount (Table1) most probably is due to a material structure change (*i.e.* missing cluster defects, the porosity changes, etc.).

N_2 adsorption-desorption isotherms

The N_2 isotherms for ZrMOF samples with or without acetic acid are presented in Figure 3. After IUPAC (Thommes et al. 2015) the recorded isotherms are type Ib and IV and the materials exhibits micropores and mesopores.

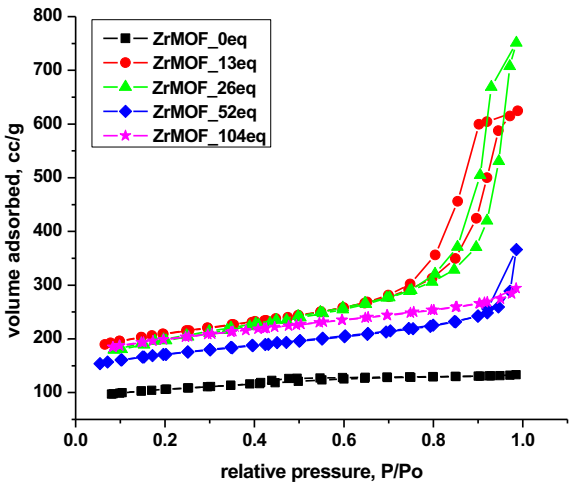

Figure 3. N_2 adsorption-desorption isotherms of ZrMOF samples

The sample ZrMOF_0eq with free AAc presents a type IVa isotherm, specific to capillary condensation, accompanied by H4 type hysteresis. The hysteresis loop H4 is specific to mesoporous materials associated with a small percent of microporosity. When acetic acid was added, the isotherms start to modify. In case of sample ZrMOF_13eq the isotherm is type IVa with H2b) hysteresis. The H2b) type of hysteresis loop is characteristic for complex pore with larger neck widths associated with pore blocking model. For these loops, the sample exhibited a plateau at the desorption branch which surpassed the plateau recorded for the adsorption branch. ZrMOF_26eq presented a type IVa isotherm with H1 hysteresis. This type of hysteresis is associated with ink-bottle pores where the width of the neck size distribution is similar to the width of the pore/cavity size distribution (Thommes et al. 2015). For samples with 52eq and 104eq of AAc, the isotherm shows the type Ib isotherm. This type of isotherm is characteristic for the materials that contain a small amount of mesopores and the majority part are micropores.

Table 2. Textural parameters

Samples	*1*	*2*	*3*	*4*	*5*
ZrMOF_0eq	*4.57*	*373*	*261*	*0.20*	*0.11*
ZrMOF_13eq	*18.55*	*741*	*484*	*0.96*	*0.21*
ZrMOF_26eq	*28.36*	*703*	*382*	*1.16*	*0.17*
ZrMOF_52eq	*27.37*	*607*	*417*	*0.57*	*0.18*
ZrMOF_104eq	*3.77*	*692*	*486*	*0.46*	*0.22*

1 - DFT, Pore diameter [nm]; 2 - BET, surface area [m^2/g]; 3 - V-t method, Micropore area [m^2/g]; 4 - Total pore volume[cm^3/g], 5 - Alpha-S, Micropore volume [cc/g]

The specific surface area (calculated with BET method) of the materials almost doubles with the addition of the organic modulator; the highest surface area (741 m^2/g) being registered for the sample with 13eq of acetic acid with a total pore volume of 0.96 cc/g (Table 2). ZrMOF_26eq shows a surface area (703 m^2/g) smaller than the previous sample, but a higher total volume of pores, with a value of 1.16 cc/g. The specific surface area continues to decrease to 607 m^2/g for ZrMOF_52eq with a halved value of total pore volume of 0.57 cc/g. Increasing the concentration of the modulator to 104 eq, an increase of surface area was observed (692 m^2/g) with a total pore volume of 0.46 cc/g, this means that for a certain limit of the modulator concentration, the specific surface area decreases and then above this limit it starts to increase again.

Absence of modulator seems to alter the mesoporous network of the material up to a point where cavitation take place (Thommes et al. 2015). Also, acetic acid in excess (sample ZrMOF_104eq) may degrade the material and even if the porosity increases, more micropores are formed at the expense of mesopores. However, all the samples studied here have a surface area smaller than those recorded for UIO-66 samples (Wu et al. 2013).

The pore size distribution obtained with DFT method is presented in Fig. 4.

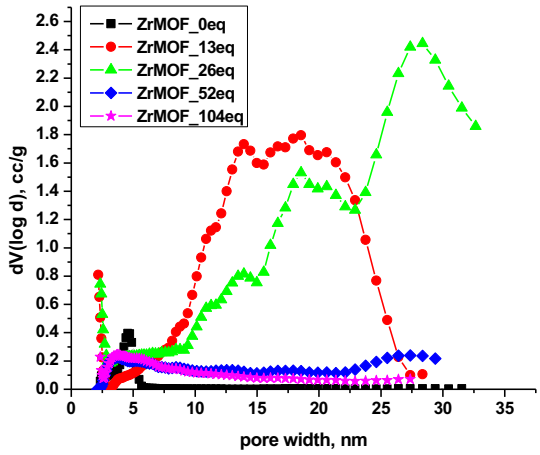

Figure 4. Pore size distribution

From Figure 4, can be observed that in case of sample with 0eq, 52eq and 104eq of AAc, the material presents a wider unimodal distribution in the micropore and mesopore region, with pore diameter of almost 4 nm (for 0eq and 104eq) and 27 nm (for 52eq), calculated with DFT method. For sample with 13eq of AAc, the material presents a bimodal distribution with larger pores of 18 nm. We observe an increase in pore width up to sample ZrMOF_26eq becoming multimodal distribution with a diameter of pores of 28 nm.

In Figure 5 is presented the microporosity percent calculated with Alpha-S method.

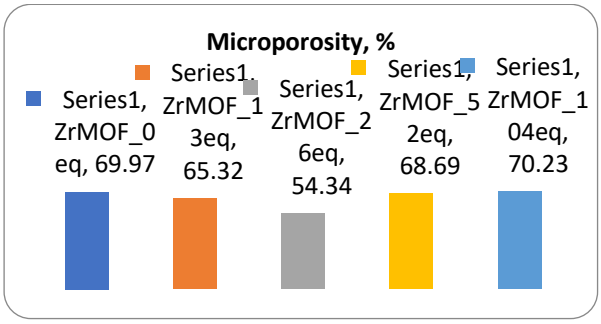

Figure 5. Microporosity percent calculated with Alpha-S method

It can be observed that the highest mesoporosity percent was obtained for sample ZrMOF_26eq. The highest content of microporosity was observed for sample without AAc and sample with the highest content of AAc with a value of ~70%.

CONCLUSIONS

In summary, we have carried out a short study of modulator effects on the surface area of some zirconium metal-organic frameworks based on terephtalic acid, in excess of Zr(IV) precursor salt. Based on thermogravimetric analysis, increasing the modulator concentration resulted in more hygroscopic materials with some missing linker defects. The presence of these defects was investigated by nitrogen adsorptions-desorption isotherms. An improvement of surface area and a change of pore structure by producing mesopores at the expense of micropores were observed in the presence of modulator. However, the amount of modulator should be carefully chosen to control the surface area, pore volume and type of porosity.

In conclusion, the insertion of a modulator during synthesis and its removal by activation process generates materials with missing linker/cluster defects even in condition of metal salt precursor excess. We showed that an increase in the concentration of modulator up to a certain value leads to an improvement of surface area and a modification of pore structure by producing mesopores at the expense of micropores.

ACKNOWLEDGEMENTS

This work was supported by the Romanian Academy, Project 4.1.

REFERENCES

Angeli, G.K., Batzavali, D., Mavronasou, K., Tsangarakis, C., Stuerzer, T., Ott, H., Trikalitis, P.N., 2020. Remarkable Structural Diversity between Zr/Hf and Rare-Earth MOFs via Ligand Functionalization and the Discovery of Unique (4,8)-c and (4, 12)-connected Frameworks. J. Am. Chem. Soc. 142, 15986−15994. https://doi.org/10.1021/jacs.0c07081

Ardila-Suarez, C., Rodríguez-Pereira, J., Baldovino-Medrano, V.G., Ramírez-Caballero, G.E., 2019. An Analysis of the Effect of the Zirconium Precursor of MOF-808 on its Thermal Stability, Structural and Surface Properties. Cryst. Eng. Comm. 21, 1407−1415. https://doi.org/10.1039/C8CE01722K

Bai, Y., Dou, Y., Xie, L.-H., Rutledge, W., Li, J.-R. Zhou, H.-C., 2016. Zr-based metal–organic frameworks: design, synthesis, structure, and applications. Chem. Soc. Rev. 45, 2327. https://doi.org/10.1039/C5CS00837A

Brunauer, S., Emmett, P.H., Teller, E., 1938. Adsorption of Gases in Multimolecular Layers. J. Am. Chem. Soc. 60(2), 309−319. https://doi.org/10.1021/ja01269a023

Cavka, J.H., Jakobsen, S., Olsbye, U., Guillou, N., Lamberti, C., Bordiga, S., Lillerud, K.P., 2008. A new zirconium inorganic building brick forming metal organic frameworks with exceptional stability. J. Am. Chem. Soc. 130, 42, 13850–13851. https://doi.org/10.1021/ja8057953

Chang, Z., Li, F., Qi, X., Jiang, B., Kou, J., Sun, C., 2020. Selective and Efficient Adsorption of Au (III) in aqueous solution by Zr-based metal-organic frameworks (MOFs): An unconventionally way for gold recycling. J. Hazard. Mater. 391, 122175. https://doi.org/10.1016/j.jhazmat.2020.122175

Chen, Z., Hanna, S.L., Redfern, L.R., Alezi, D., Islamoglu, T., Farha, O.K., 2019. Reticular chemistry in the rational synthesis of functional zirconium cluster-based MOFs. Coord. Chem. Rev. 386, 32–49. https://doi.org/10.1016/j.ccr.2019.01.017

Chen, Z., Feng, L., Liu, L., Bhatt, P.M., Adil, K., Emwas, A.-H., Assen, A.H., Belmabkhout, Y., Han, Y., Eddaoudi, M., 2018. Enhanced Separation of butane Isomers via Defect Control in Fumarate/Zirconium-Based Metal Organic Framework. Langmuir 34, 48, 14546−14551. https://doi.org/10.1021/acs.langmuir.8b03085

Drout, R.J., Robison, L., Chen, Z., Islamoglu, T., Farha, O.K., 2019. Zirconium Metal–Organic Frameworks for Organic Pollutant Adsorption, Trends Chem., 1(3), 304−3017. https://doi.org/10.1016/j.trechm.2019.03.010

Fang, X., Zong, B., Mao, S., 2018. Metal–Organic Framework-Based Sensors for Environmental Contaminant Sensing. Nano-Micro Lett. 10, 64. https://doi.org/10.1007/s40820-018-0218-0

Feng, D., Wang, K., Wei, Z., Chen, Y.P., Simon, C.M., Arvapally, R.K., Martin, R.L., Bosch, M., Liu, T.-F., Fordham, S., Yuan, D., Omary, M.A., Haranczyk, M., Smit, B., Zhou, H.-C., 2015. Kinetically Tuned Dimensional Augmentation as a Versatile Synthetic Route towards Robust Metal–organic Frameworks. Nat. Commun. 6, 6106. https://doi.org/10.1038/ncomms7106

Ghanbari, T., Abnisa, F., Wan Daud, W.M.A., 2020. A review on production of metal organic frameworks (MOF) for CO2 Adsorption. Sci. Total Environ. 707, 135090. https://doi.org/10.1016/j.scitotenv.2019.135090

Guan, T., Li, X., Fang, W., Wu, D., 2020. Efficient removal of phosphate from acidified urine using UIO-66 metal-organic frameworks with varying functional groups. Appl. Surf. Sci. 501, 144074.

https://doi.org/10.1016/j.apsusc.2019.144074
Han, X., Godfrey, H.G.W., Briggs, L., Davies, A.J., Cheng, Y., Daemen, L.L., Sheveleva, A.M., Tuna, F., McInnes, E.J.L., Sun, J., Drathen, C., George, M.W., Ramirez-Cuesta, A.J., Thomas, K.M., Yang, S., Schröder M., 2018. Reversible adsorption of nitrogen dioxide within a robust porous metal–organic framework, Nat. Nat. 17(8), 691−696.
https://doi.org/10.1038/s41563-018-0104-7
Han, Y., Liu, M., Li, K., Zuo, Y., Wei, Y., Xu, S., Zhang, G., Song, C., Zhang, Z.C., Guo, X., 2015. Facile synthesis of morphology and size-controlled zirconium metal–organic framework UiO-66: the role of hydrofluoric acid in crystallization. Cryst. Eng. Comm. 17, 6434−6440.
https://doi.org/10.1039/C5CE00729A
Helal, A., Cordova K.E., Arafat, E., Usman, M., Yamani Z.H., 2020. Defect-engineering a metal–organic framework for CO2 fixation in the synthesis of bioactive oxazolidinones. Inorg. Chem. Front. **7**, 3571−3577.
https://doi.org/10.1039/D0QI00496K
Hu, Z., Peng, Y., Kang, Z., Qian, Y., Zhao, D., 2015. A Modulated Hydrothermal (MHT) Approach for the Facile Synthesis of UiO-66-Type MOFs. Inorg. Chem. 54(10), 4862−4868.
https://doi.org/10.1021/acs.inorgchem.5b00435
Jiang, K., Zhang, L., Hu, Q., Zhang X., Zhang, J., Cui, Y., Yang, Y., Li, B., 2019. Guodong Qian, A Zirconium-based Metal-organic Framework with Encapsulated Anionic Drug for Uncommonly Controlled Oral Drug Delivery. Microporous Mesoporous Mater. 275, 229−234.
https://doi.org/10.1016/j.micromeso.2018.08.030
Kalaj, M., Prosser, K.E., Cohen, S.M., 2020. Room Temperature Aqueous Synthesis of UiO-66 Derivatives via Postsynthetic Exchange, Dalton Trans. 49, 8841-8845.
https://doi.org/10.1039/D0DT01939A
Kirlikovali, K.O., Chen, Z., Islamoglu, T., Hupp, J.T., Farha, O.K., 2020. Zirconium-Based Metal−Organic Frameworks for the Catalytic Hydrolysis of Organophosphorus Nerve Agents. ACS Appl. Mater. Interfaces 120, 16, 8130–8160.
https://doi.org/10.1021/acsami.9b20154
Li, B., Chrzanowski, M., Zhang, Y., Ma, S., 2016. Applications of metal-organic frameworks featuring multi-functional sites. Coord. Chem. Rev. 307, 106–129.
https://doi.org/10.1016/j.ccr.2015.05.005
Li, H.Y., Xu, J., Li, L.K., Du, X.S., Li, F.A., Xu, H., Zang, S.Q., 2017. Photochromic Properties of a Series of Zn(II)-Viologen Complexes with Structural Regulation by Anions. Cryst. Growth Des. 17, 6311–6319.
https://doi.org/10.1021/acs.cgd.7b00995
Li, B., Zhua, X., Hu, K., Li, Y., Feng, J., Shi, J., Gu, J., 2016. Defect creation in metal-organic frameworks for rapid and controllable decontamination of roxarsone from aqueous solution. J. Hazard. Mater. 302, 57–64.
https://doi.org/10.1016/j.jhazmat.2015.09.040
Liu, S., Bai, J., Huo, Y., Ning, B., Peng, Y., Li, S., Han, D., Kang, W., Gao, Z., 2020. A zirconium-porphyrin MOF-based ratiometric fluorescent biosensor for rapid and ultrasensitive detection of chloramphenicol. Biosens. Bioelectron. 149, 111801.
https://doi.org/10.1016/j.bios.2019.111801
Pan, D., Jaroniec, M., Klinik, J., 1996. Thermogravimetric evaluation of the specific surface area and total porosity of microporous carbons. Carbon 34(9), 1109−1113.
https://doi.org/10.1016/0008-6223(96)00063-2
Piszczek, P., Radtke, A., Grodzicki, A., Wojtczak, A., Chojnacki, J., 2007. The new type of [Zr6(μ3-O)4(μ3-OH)4] cluster core: Crystal structure and spectral characterization of [Zr6O4(OH)4(OOCR)12] (R=But, C(CH3)2Et). Polyhedron 26(3), 679−685.
https://doi.org/10.1016/j.poly.2006.08.025
Ravikovitch, P.I., O'Domhnaill, S.C., Neimark, A.V., Schuth, F., Unger, K.K., 1995. Capillary hysteresis in nanopores: theoretical and experimental studies of nitrogen adsorption on MCM-41, Langmuir 11, 4765–4772.
https://doi.org/10.1021/la00012a030
Ren, J., Ledwaba, M., Musyoka N.M., Langmi, H.W., Mathe, M., Liao, S., Pang W., 2017. Structural defects in metal–organic frameworks (MOFs): Formation, detection and control towards practices of interests. Coord. Chem. Rev. 349, 169–197.
https://doi.org/10.1016/j.ccr.2017.08.017

Schaate, A., Roy, P., Godt A., Lippke, J., Waltz, F, Wiebcke, M., Behrens, P., 2011. Modulated Synthesis of Zr-Based Metal–Organic Frameworks: From Nano to Single Crystals, Chem. Eur. J. 17, 6643–6651. https://doi.org/10.1002/chem.201003211

Seetharaj, R., Vandana, P.V., Arya, P., Mathew, S., 2019. Dependence of solvents, pH, molar ratio and temperature in tuning metal organic framework architecture. Arab. J. Chem. 12, 295–315. https://doi.org/10.1016/j.arabjc.2016.01.003

Sharmin, E., Zafar, F., 2016. Introductory Chapter: Metal Organic Frameworks (MOFs), Metal-Organic Frameworks, Edited by Zafar, F. and Sharmin, E., IntechOpen. https://dx.doi.org/10.5772/64797

Shearer, G.C., Chavan, S., Bordiga, S., Svelle, S., Olsbye U., Lillerud K.P., 2016. Defect Engineering: Tuning the Porosity and Composition of the Metal–Organic Framework UiO-66 via Modulated Synthesis. Chem. Mater. 28, 3749−3761. https://doi.org/10.1021/acs.chemmater.6b00602

Silverstein, R.M., Webster, F.X., 1998. Spectrometric identification of organic compounds, Sixth Ed., John Wiley & Sons, Inc., New York, USA

Su, J., Yuan, S., Wang, T., Lollar, C., Zuo, J., Zhang, J., Zhou, H., 2020. Zirconium Metal-organic frameworks Incorporating Tetrathiafulvalene Linkers: Robust and Redox-Active Matrices For In Situ Confinement of Metal Nanoparticles. Chem. Sci. 11, 1918–1925. https://doi.org/10.1039/C9SC06009J

Taddei, M., 2017. When defects turn into virtues: The curious case of zirconium-based metal-organic frameworks. Coord. Chem. Rev. 343, 1–24. https://doi.org/10.1016/j.ccr.2017.04.010

Thommes, M., Kaneko, K., Neimark, A.V., Olivier, J.P., Rodriguez-Reinoso, F., Rouquerol, J., Sing, K.S.W., 2015. Physisorption of gases, with special reference to the evaluation of surface area and pore size distribution (IUPAC Technical Report). Pure Appl. Chem. 87(9-10), 1051–1069. https://doi.org/10.1515/pac-2014-1117

Wang, S.L., Hu, F.L., Zhou, J.Y., Zhou, Y., Huang, Q., Lang, J.P., 2015. Rigidity versus Flexibility of Ligands in the Assembly of Entangled Coordination Polymers based on Bi and Tetra Carboxylates and N-Donor Ligands. Cryst. Growth Des. 15, 4087–4097. https://doi.org/10.1021/acs.cgd.5b00642

Wang, B., Wang, P., Xie, L.-H., Lin, R.-B., Lv, J., Li, J.-R., Che, B., 2019. A Stable Zirconium based Metal-Organic Framework for Specific Recognition of Representative Polychlorinated Dibenzo-p-dioxin Molecules. Nat. Commun. 10, 3861. https://doi.org/10.1038/s41467-019-11912-4

Wang, Y., Li, L., Dai, P., Yan, L., Cao, L., Gu, X., Zhao, X., 2017. Missing-node directed synthesis of hierarchical pores on a zirconium metalorganic framework with tunable porosity and enhanced surface acidity via a microdroplet flow reaction. J. Mater. Chem. A 5(42), 22372–22379. https://doi.org/10.1039/C7TA06060B

Winarta, J., Shan, B., Mcintyre, S.M., Ye, L., Wang, C., Liu, J., Mu, B., 2020. A Decade of UiO-66 Research: A Historic Review of Dynamic Structure, Synthesis Mechanisms, and Characterization Techniques of an Archetypal Metal−Organic Framework. Cryst. Growth Des. 20, 1347−1362. https://doi.org/10.1021/acs.cgd.9b00955

Xiong, Y., Fang, Y.Z., Borges, D.D., Chen, C.X., Wei, Z.W., Wang, H.P., Pan, M., Jiang, J.J., Maurin, G., Su, C.Y., 2016. Ligand and Metal Effects on the Stability and Adsorption Properties of an Isoreticular Series of Mofs Based on T-shaped Ligands and Paddle-Wheel Secondary Building Units. Chem. Eur. J. 22, 16147–16156. https://doi.org/10.1002/chem.201603299

Yao, S.-L., Liu, S.-J., Cao, C., Tian, X.-M., Bao, M.-N., Zheng, T.-F., 2019. Temperature- and Solvent-Dependent Structures of Three Zn(II) Metal-Organic Frameworks for Nitroaromatic Explosives Detection. J. Solid State Chem. 269, 195–202. https://doi.org/10.1016/j.jssc.2018.09.032

Yang, F., Li, W., Tang B., 2018. Facile synthesis of amorphous UiO-66 (Zr-MOF) for supercapacitor application. J. Alloys Compd. 733, 8–14. https://doi.org/10.1016/j.jallcom.2017.10.129